Influence of gas flow velocity on the transport of chemical species in an atmospheric pressure air plasma discharge

M. I. Hasan and J. L. Walsh

Citation: Appl. Phys. Lett. **110**, 134102 (2017); doi: 10.1063/1.4979178
View online: http://dx.doi.org/10.1063/1.4979178
View Table of Contents: http://aip.scitation.org/toc/apl/110/13
Published by the American Institute of Physics

Influence of gas flow velocity on the transport of chemical species in an atmospheric pressure air plasma discharge

M. I. Hasan and J. L. Walsh[a)]
Centre for Plasma Microbiology, Department of Electrical Engineering and Electronics, the University of Liverpool, Brownlow Hill, Liverpool L69 3GJ, United Kingdom

(Received 19 December 2016; accepted 14 March 2017; published online 29 March 2017)

This paper reports on a numerical study of the transport of reactive chemical species generated in an atmospheric-pressure air plasma discharge under the influence of a high velocity flowing gas. Using a 1D air plasma model, it is shown that the reactive species transported downstream of the discharge region can be categorized into three distinct groups based on their spatial distribution: (i) decaying downstream species, (ii) increasing downstream species and (iii) variable density species, where the density is a function of both spatial position and gas flow velocity. It is demonstrated that the gas flow velocity influences the dominant chemical reactions downstream of the discharge region, noticeably altering the composition of several key reactive chemical species transported to a given downstream location. As many emerging applications of atmospheric pressure plasma are driven by the flux of reactive chemical species, this study highlights the importance of gas flow velocity, not only as a means to enhance mass transport but also as a means to manipulate the very nature of the reactive plasma chemistry arriving at a given location. [http://dx.doi.org/10.1063/1.4979178]

Atmospheric-pressure air plasma discharges (AAPDs) generated in humid air are used extensively in the fields of materials modification[1,2] and environmental remediation[3] due to their convenience and low cost. Recently, the use of such plasmas in biomedical applications has grown rapidly due to their unique ability to generate a wealth of highly reactive chemical species directly at the point of need, using only air and electricity. Typical applications where AAPD has shown great promise include microbial decontamination,[4] cancer treatment,[5] and wound healing.[6] Critically, all the aforementioned applications are primarily driven by the flux of reactive chemical species arriving at the sample surface. Maximizing the efficiency of an AAPD in a given application often goes beyond simply delivering a large and indiscriminate flux of reactive species to the sample but requires the composition of specific species to be increased, while others are reduced. The ability to tailor the species composition of an AAPD is particularly challenging given the constraint of working in ambient air and the complexity of the underpinning physical and chemical processes.

A major challenge in optimizing AAPDs for a particular application is the inability to fully characterize the generated reactive species using current experimental techniques. Infra-red Fourier transform (FTIR) spectroscopy has been widely used but can only detect chemical species that actively absorb infra-red radiation.[7] Laser-induced fluorescence (LIF) is also used extensively for quantification of plasma generated species but suffers due to high quenching rates in air at atmospheric pressure.[8] Given the complexities of experimental characterization, numerical modelling provides an alternate means to explore the complex chemistry produced in an AAPD. Through numerical modelling, the underpinning production pathways of key plasma generated species can be identified, an essential precursor in understanding how a discharge chemistry can be tailored for a given application.

In this paper, a numerical study is presented highlighting the influence of relatively high flow velocities (>1 m/s) on the reactive species generated and transported in an AAPD. The numerical model used in the study solves a coupled set of 1D convection-diffusion-reaction equations. These are solved for 53 species including electrons, positive and negative ions, excited state neutral species and neutral reactive species, interacting through 624 reactions. A complete list of the species and reactions considered was reported by Sakiyama and co-workers.[9] The background air is assumed to consist of 97% N_2, 20% O_2 and 1% H_2O. The model solves for the mass fractions of all species as a function of space and time. The electric field driving the discharge is modelled as a Gaussian pulse with a duration of a few nanoseconds, mimicking the lifetime of a filamentary discharge; this field is converted into a mean electron energy of electrons through the local field approximation.[9] More details on the model can be found in Ref. 10. Two major enhancements have been added to the model in this work. The first enhancement is the introduction of a convective flux term to the mass continuity equation solved for every species except electrons, assuming a constant velocity everywhere in the domain. This modification extends the validity of the model to higher flow velocities ($>1\,m\,s^{-1}$). The second enhancement involves accounting for the ambipolar electric field. This is done by solving the Poisson equation in the domain for the electric potential and then adding an electric field-driven flux to the total flux of every charged species. The potential is set equal to zero at $x = 0$ cm as a boundary condition for the Poisson equation. This condition implies

[a)]Author to whom correspondence should be addressed. Electronic mail: jlwalsh@liv.ac.uk

that the potential in the computation domain is taken with respect to the plasma potential at x = 0 cm, which is assumed to be zero. The boundary condition at the other end of the domain, x = 5 cm, is set to $E_x = 0$. With respect to the system of equations solved in the model, the boundary condition assumed at both ends of the computational domain is an outflow condition, which sets the outward flux from the domain equal to the sum of the convective and the electric field-driven fluxes at the boundary points.

The plasma was assumed to consist of 15 ns streamers generated at a repetition frequency of 30 kHz, this represents the positive and negative half cycles of an applied voltage waveform with a period of 66.67 μs. The deposited power density was set to 500 W cm^{-2}. Such conditions match those found in many reported experimental studies of surface barrier discharge (SBD) systems operating in air at atmospheric pressure.[11,12] It is well known that the seemingly uniform discharge comprises a large number of short-lived streamers propagating along the dielectric surface; typical power densities range from 100 to 1000 W cm^{-2} (Refs. 9 and 12).

For every flow velocity assumed, 50 periods were solved. While solving, the applied electric field was regulated to maintain the computed power density within 5% of the 500 W cm^{-2} target. For all cases investigated, the computed power density arrived to within +/− 5% of the deposited power density within 5 periods.

The model was run for four flow velocity cases, v_f = 3 m s^{-1}, 6 m s^{-1}, 12 m s^{-1}, and 24 m s^{-1}. The rationale for this choice was motivated by recent experimental studies, where SBD systems have be shown to operate with flow velocities approaching 10 m s^{-1}[13] and air plasma jets that can operate at flow velocities above 20 m s^{-1} (Ref. 14). In all cases, the results showed that short lived species such as $N_2(A^3)$, $N_2(B^3)$, $N(^2D)$, $O(^1D)$, H, electrons, and most positive and negative ions have short lifetimes, and the increased flow does not significantly influence their behavior. Consequently, such species are confined to the discharge region (at x = 0) and only the behavior of the longed lived species is discussed.

The spatial distributions of long-lived species at the end of the 50th period can be identified as falling into one of the three distinct categories: (1) Decaying downstream species, where the density of the species decrease downstream; this category includes OH, $O_2(a^1\Delta)$, and N. (2) Increasing downstream species, where the density of the species increases downstream; this category includes NO_2, HNO_2, HNO_3, N_2O, H_2O_2 and O_3. (3) Varying density species, where the density fluctuates as the species are transported in the downstream direction; this category includes HO_2 and NO. The time-averaged density profiles observed after the 50th period for the 3 categories are shown for the v_f = 3 m s^{-1} case in Figure 1 up to 2 cm of the computational domain.

The species behaviour shown in Figure 1 can be explained by examining the net reaction rates of all species, as given by

$$R = \sum_g A_g R_g - \sum_l B_l R_l, \quad (1)$$

where R is the net reaction coefficient. The first sum in (1) captures the gain components, where A_g and R_g are the stoichiometric coefficient and the reaction rate of the generating reactions, respectively. The second sum in (1) captures the loss reactions, where B_l and R_l are the stoichiometric coefficient and the reaction rate of the loss reactions, respectively.

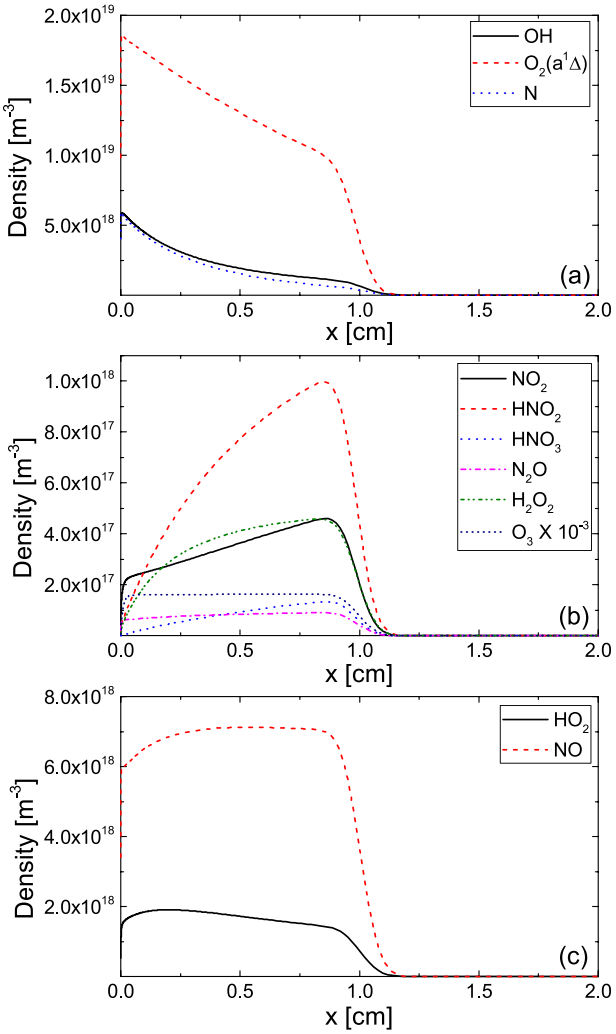

FIG. 1. The species densities at the end of the 50th period for a flow velocity of 3 m s^{-1}. Only 0–2 cm of the computation domain is shown for clarity.

For the decaying downstream species, the negative component of R is much greater than the positive component, indicating they are consumed as they are transported downstream. The opposite is true for the increasing downstream species, as shown in Figure 1(b), where the positive component of R is much greater than the negative component, indicating that the species are being generated as they are transported downstream. For the varying density species, the positive and negative components of R are comparable, resulting in a net reaction rate that varies downstream as a function of distance. Typically, for these species, R is positive close to the plasma region and becomes negative further downstream, explaining the trends observed in Figure 1(c). The ratio between the positive and the negative components of R for NO ranges between 0.5 and 1.4, while the difference between those for decaying and growing downstream species are the different by 1–2 orders of magnitude.

In many applications, reactive oxygen and nitrogen species (RONS) such as OH radicals are considered to be of

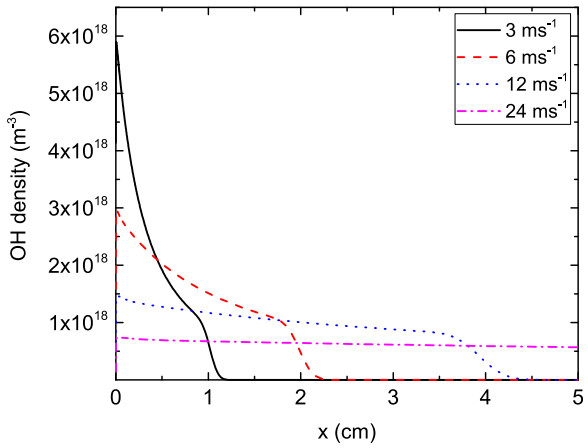

FIG. 2. The OH density at the end of the 50th period for different flow velocities.

paramount importance, yet it is often assumed that their transport downstream of an air plasma is limited due to a short lifetime. Figure 2 shows the time-averaged OH density at different flow velocities. It is clear from Figure 2 that the distance over which OH is distributed is directly proportional to the flow velocity in a given time interval. It is also clear that the OH density at a given point in the domain is inversely proportional to the flow velocity. This can be explained by the fact that the amount of OH generated in the plasma region in every period at a constant operating power is essentially constant, regardless of the flow velocity. When the flow velocity is doubled, the total generated OH density is spread over twice the distance, resulting in a lower local OH density at a given location. Critically, this variation in density is influenced not only by the transport of species downstream but also due to the modification of the generation and loss rates of the various species.

To evaluate the impact of the flow velocity on the chemical reactions, the species densities are spatially averaged over the computational domain at the end of the 50th period. These space-averaged densities are reported as a function of the flow velocity in Table I. The 24 m s^{-1} case has been omitted in the table because species exit the computational domain, making this case incomparable to the others. From Table I, a clear trend can be observed whereby the space-averaged densities of the decaying downstream group of species increase with flow velocity, while the averaged densities of the increasing downstream group of species decrease with flow velocity. This is a significant factor for several key species including OH, H_2O_2, NO_2, and HNO_3. These observations are attributed to two coupled factors: the first of which is increased convection, which in turn influences the chemical reaction rates that are the second factor behind these trends.

TABLE I. The space-averaged densities for $v_f = 3$ m s^{-1}, 6 m s^{-1}, and 12 m s^{-1}. The 24 m s^{-1} case is excluded because the densities are spread over a distance greater than the computational domain.

Species	3 m s^{-1}	6 m s^{-1}	12 m s^{-1}	Category
$O_2(a^1\Delta)$	2.7×10^{18}	2.9×10^{18}	3.2×10^{18}	Decaying downstream
OH	4.7×10^{17}	6.6×10^{17}	8.3×10^{17}	
N	3.9×10^{17}	5.1×10^{17}	5.4×10^{17}	
NO	1.4×10^{18}	1.6×10^{18}	1.5×10^{18}	Variable density
HO_2	3.4×10^{17}	3.5×10^{17}	3.3×10^{17}	
O_3	3.2×10^{19}	3.1×10^{19}	3.1×10^{19}	Increasing downstream
NO_2	7.2×10^{16}	6×10^{16}	4.7×10^{16}	
H_2O_2	7.4×10^{16}	5.9×10^{16}	4.4×10^{16}	
HNO_2	1.4×10^{17}	1.1×10^{17}	7×10^{16}	
HNO_3	1.7×10^{16}	1.1×10^{16}	6.1×10^{15}	
N_2O	1.6×10^{16}	1.5×10^{16}	1.3×10^{16}	

To understand the influence of convection, the continuity equation for an arbitrary species is given in Equation (2). For the flow velocities considered in this work, the convective flux dominates over the diffusive flux. Given that the velocity field is assumed constant, the divergence of the flux term in Equation (2) can be written explicitly, moved to the right hand side, as shown in Equation (3).

$$\frac{\partial n}{\partial t} + \nabla \cdot \vec{\Gamma} = R, \tag{2}$$

$$\frac{\partial n}{\partial t} = R - v_f \frac{\partial n}{\partial x} = R + R_{eff}, \tag{3}$$

where n is the density of an arbitrary species, Γ is the net flux of that species and R is the net reaction rate. Equation (3) shows that convection can be considered as an effective reaction term R_{eff} that is similar in nature to R. This formulation localizes convection, making it possible to consider every point in the computational domain as an independent batch reactor. For all the flow velocities investigated in this work, there is a semi-balance between R_{eff} and R in the downstream region, which minimizes the time change in density in the downstream regions of the domain.

For the decaying downstream species, the spatial derivative is negative; thus, R_{eff} becomes positive that adds to the negative R for decaying downstream species. Consequently, the loss rate of these species becomes smaller and their life-time is extended, explaining the increase in the space-averaged densities listed in Table I. This scenario also holds true for increasing downstream species, and the spatial derivative is positive making R_{eff} negative, which subtracts from the positive R, causing a decrease in the total generation rate of these species, which is responsible for the drop in their space-averaged densities, as highlighted in Table I. Notably, the space-averaged density of O_3 deviates from this trend and is attributed to the relatively flat density profile of O_3 shown in Figure 1(b), making the spatial derivative small and R_{eff} small as well.

For the variable density category, the influence of convection is more complex as the influence of R_{eff} on the density varies with both the flow velocity and position. For regions where R is positive, which is close to the plasma region, the effective reaction rate decreases the growth rate. For distances further downstream, R is negative and the effective reaction rate lowers their loss rate. Consequently, the change of their space-averaged densities as a function of flow velocity is not monotonic. The increase in the space-averaged density from 3 m s^{-1} to 6 m s^{-1} occurs because the negative component of R is weakened. This behaviour has a major influence on certain species, such as NO and HO_2, as

R becomes positive everywhere in the domain resulting in increased space-averaged density of both species.

Since the net reaction rate R and the effective reaction rate R_{eff} are coupled, it is expected that the presence of R_{eff} will change the behaviour of R. This is particularly important for four key species: OH, H_2O_2, NO_2, and HNO_3. In the case of OH, a dominant loss pathway is $2OH + M \rightarrow H_2O_2 + M$, which corresponds to a loss term in the OH conservation equation of the form $-kn_{OH}^2$, where k is the reaction coefficient and n_{OH} is the OH density. The time dependence corresponding to this quadratic loss term is of the form $\frac{n_0}{n_0kt+1}$, where n_0 is the initial density. Unlike exponential decay terms, where the decay rate or lifetime is independent of the density, this term has a decay rate that becomes smaller for lower densities. Higher flow velocities result in a lower density at a given point in space, meaning the intensity of this loss reaction becomes weaker for higher flow velocities. This behaviour, combined with the effects of increased convection represented by R_{eff}, extends the lifetime of OH and thus increases its space-averaged density. Given that this OH loss reaction is the main generation pathway for H_2O_2, it is clear to see why a drop in the space-averaged density of H_2O_2 occurs as flow velocity increases.

For NO_2, one of the dominant generation pathways is $NO + HO_2 \rightarrow NO_2 + OH$: near the plasma region, the density of reactants decreases as a result of convection; hence, less NO_2 is generated there. This has a knock-on effect on the space-averaged density of HNO_3 that is generated through the reaction between NO_2 and OH as follows: $NO_2 + OH + M \rightarrow HNO_3 + M$. As the space-averaged density of NO_2 drops with increasing velocity, the space-averaged density of HNO_3 also drops.

This paper provides insights into the behavior of reactive species transport in an atmospheric pressure air plasma discharge under the influence of a flowing gas using a 1D computational model. Based on the spatial distribution of the reactive species produced, three distinct groups can be identified. One group of species shows a collective decay as they are transported downstream of the discharge region, including, for example, OH, $O_2(a^1\Delta)$, and N. A second group of species is observed to increase in density, as they are transported downstream, including, for example, NO_2, HNO_3, N_2O, H_2O_2, and O_3. Finally, a third group of species is identified that vary in density with position and flow velocity, including, for example, NO and HO_2.

It is demonstrated that increased convection affects the decaying downstream species by weakening their loss processes, extending their life time and increasing their space-averaged densities. Conversely, convection weakens the generation processes of the increasing downstream group of species, causing their space-averaged densities to decrease. In essence, convection can be seen as a means to slow the chemical reactions downstream, extending the lifetimes of highly reactive species such as OH at the expense of more stable species such as NO_2. From a practical perspective, these findings have important implications, as it is the highly reactive short-lived species that have the greatest impact on the efficacy of a given application. A typical example of this is in the use of AAPD for microbial decontamination, where oxidative stress caused by short lived plasma generated species such as OH is primarily responsible for the antimicrobial effects observed.[15] This work indicates that an AAPD could be tailored for such applications by manipulating the convection velocity to increase the flux of short-lived species arriving at a given downstream point.

The authors are thankful for the support of the UK Engineering and Physical Sciences Research Council (Project EP/N021347/1) and Innovate UK (Project 50769-377232). J.L.W. also acknowledges the support from NATO (Grant SPS.984555).

[1]H. Zhang, H. Li, M. Fang, Z. Wang, L. Sang, L. Yang, and Q. Chen, Appl. Surf. Sci. **388**, 539 (2016).
[2]J. Leea, S. Hwanga, D.-H. Choa, J. Hong, J. H. Shinb, and D. Byun, Appl. Surf. Sci. **394**, 543 (2017).
[3]M. Magureanu, N. B. Mandache, and V. I. Parvulescu, Water Res. **81**, 124 (2015).
[4]D. Wang, D. Zhao, K. Feng, X. Zhang, D. Liu, and S. Yang, Appl. Phys. Lett **98**, 161501 (2011).
[5]H. Tanaka, M. Mizuno, K. Ishikawa, H. Kondo, K. Takeda, H. Hashizume, K. Nakamura, F. Utsumi, H. Kajiyama, and H. Kano, Clin. Plasma Med. **3**, 72 (2015).
[6]D. W. Kim, T. J. Park, S. J. Jang, S. J. You, and W. Y. Oh, Appl. Phys. Lett. **109**, 233701 (2016).
[7]P. Atkins and J. de Paula, *Physical Chemistry*, 9th ed. (W.H. Freeman & Co., 2009), Chap. 12.
[8]R. Ono, J. Phys. D: Appl. Phys. **49**, 083001 (2016).
[9]Y. Sakiyama, D. B. Graves, H.-W. Chang, T. Shimizu, and G. E. Morfill, J. Phys. D: Appl. Phys. **45**, 425201 (2012).
[10]M. I. Hasan and J. L. Walsh, J. Appl. Phys. **119**, 203302 (2016).
[11]P. Olszewski, J. F. Li, D. X. Liu, and J. L. Walsh, J. Hazard. Mater. **279**, 60 (2014).
[12]M. J. Pavlovich, D. S. Clark, and D. B. Graves, Plasma Sources Sci. Technol. **23**, 065036 (2014).
[13]N. Benard, P. Note, M. Caron, and E. Moreau, "Highly time-resolved investigation of the electric wind caused by surface DBD at various ac frequencies," J. Electrost. (published online).
[14]J. L. Walsh and M. G. Kong, Appl. Phys. Lett. **99**, 081501 (2011).
[15]M. G. Kong, G. Kroesen, G. Morfill, T. Nosenko, T. Shimizu, J. van Dijk, and J. L. Zimmermann, New J. Phys. **11**, 115012 (2009).